INVESTIGATION OF FLOOD FORCES ON MASONRY ARCH BRIDGES USING SPH

INVESTIGATION OF FLOOD FORCES ON MASONRY ARCH BRIDGES USING SPH

Eda Majtan, Lee S. Cunningham, Benedict D. Rogers
University of Manchester
Department of Mechanical, Aerospace and Civil Engineering
Manchester M13 9PL, UK

KEYWORDS: Masonry arch bridge, flash floods, open channel flow, fluid-structure interaction, hydrostatic forces, hydrodynamic forces, computational fluid dynamics, smoothed particle hydrodynamics.

ABSTRACT

Masonry arch bridges constitute a substantial proportion of the existing bridge stock in the UK and elsewhere. Although this durable bridge form often demonstrates good structural performance under normal service loading, bridges spanning watercourses are vulnerable to damage from flood-induced loads. Fluvial flooding generates both hydrostatic and hydrodynamic effects on the arch superstructure in addition to well known-scour effects on the substructure, all of these have the potential to cause structural failure. While research on scour is relatively well advanced, quantification of the hydrodynamics forces on the bridge superstructure is not yet comprehensively understood. Where fast flood flows come into contact with the bridge superstructure, highly transient behaviour is observed, this may develop into violent interactions, particularly where floating debris is involved. This paper explores the novel use of smoothed particle hydrodynamics (SPH) to capture detailed pressure time histories and associated spatial distribution on masonry arches subject to fluvial flooding. SPH uses moving particles to represent the flow and is therefore ideal to simulate highly transient and potentially violent free-surface flows encountered during fast events. A typical arch bridge and representative flood flows are simulated in order to demonstrate the capability of the method. Under typical real-life flood flows, significant hydrodynamic pressures are generated which need to be considered in the assessment of such structures.

1. INTRODUCTION

Masonry arch bridges are among the oldest types of bridge construction and still form a major part of the bridge stock in many countries, for example, there are approximately 40,000 bridges in the UK corresponding to approximately 40% of the total stock. These historical bridges have provided efficient load-carrying capacity under vertical static and transient loads, however the combination of deterioration, ageing and weathering over time, increased traffic loads as well as man-made and natural hazards e.g., flash floods, has caused a significant number of damage or failures of masonry arch bridges throughout the UK, Ireland and other countries in Europe (Proske and Hubl, 2006; Solan et al., 2020).

Masonry arch bridges spanning rivers and canals are very vulnerable to flood-induced loads, with flash floods statistically being one of the main causes of damage and collapse (Proske, 2018). Examples of serious damage or collapse of masonry arch bridges caused by flooding in the UK over the last two decades include Braithwaite Bridge (2009), Waterstave Bridge (2012), Linton Bridge (2015), Bell Bridge (2015), Pooley Bridge (2015), Eamont Bridge (2015), Tadcaster Bridge (2015), Ballynameen Bridge (2017), Grinton Moor Bridge (July 2019) and Llanerch Bridge (2021). According to Deng et al. (2016), the main sources of bridge damage or collapse are attributed to the direct hydrodynamic action of the flood flow and/or floating debris

impact on the bridge superstructure and scour of the bridge foundation. Majtan et al. (2021) summarised the source of several bridge collapses and damages in the UK between 2009 and 2020 based on the reports published by Local and Governmental Authorities using the categories defined by Deng et al. (2016). In the case of floating debris impact, the most common source of large debris was found to be tree logs.

In flood scenarios, the forces acting on the masonry arch structure comprise horizontal hydrostatic force, hydrodynamic drag and uplift forces, buoyancy (hydrostatic uplift) force where the arch/bridge deck is submerged along with potential debris impact forces. Assessment codes for existing bridges have included the scour effect around bridge piers due to hydrodynamic actions. However, existing assessment codes provide no quantitative guidance on the flood-induced hydrodynamic forces nor floating debris impact forces on masonry arch bridges, e.g. the forthcoming UK's National Highways' assessment code CS 469 (Takano and Pooley, 2021) and its predecessor BD/97/12 (National Highways, 2012). In parallel with this, most research has focussed on scour of bridge abutments and has ignored direct hydrodynamic effects on the bridge superstructure (Witzany and Cejka, 2007; Ruocci et al., 2009; Invernizzi et al., 2011; Lamb et al., 2017; Ebrahimi et al., 2018; Prendergast et al., 2018; Solan et al., 2020). To predict the maximum waterborne debris forces on a standardised bridge deck and pier with simple geometry, US NCHRP Report 445 developed equations including the flow-blockage ratio and associated drag coefficient (Parola et al., 2000). Despite providing an insight into the debris-induced loads on a bridge structure, the study by Parola et al. (2000) did not examine the specific geometry associated with masonry arch bridges. Considering the gap in prevalent assessment codes and studies in the literature, there is a need to understand and quantify the flood-induced loads on the superstructure of masonry arch bridges (Ciria, 2017; Tubaldi et al., 2021).

The strength of masonry arch bridges subject to imposed loads is influenced by the inherent self-weight associated with the thickness of the arch barrel and the depth of the backfill. Applying Archimedes' principle to submerged components of masonry arch bridges, buoyancy forces lead to a decrease in the effective self-weight of the arch barrel and backfill and potentially reduce the load-carrying capacity of the bridge (Tubaldi et al., 2016). To determine the reduction in the load-carrying capacity due to the buoyancy forces, Hulet et al. (2006) conducted small-scale experiments considering one of the worst-case scenarios for a flooded masonry arch bridge, namely the water level at the elevation of the top of the bridge deck. The geometry of a typical segmental arch bridge in the UK was used with approximately 0.25 rise-to-span ratio, while the backfill type was quartz sand with diameters between 0.425 and 2 mm. Three fully submerged flooding cases were examined: (i) unwaterproofed bridge (ii) waterproofed bridge with external flooding and dry backfill and (iii) waterproofed bridge with internal flooding and saturated backfill, these were compared to the reference case of a dry bridge. Hulet et al. (2006) concluded that the buoyancy effect led to the reduction factor of 1.6-1.8 in the load-carrying capacity of the bridge with a submerged arch barrel and unsaturated backfill and this factor corresponded to the ratio of dry to submerged weight. To estimate flood flow, in particular the afflux which corresponds to the increase in water level of the upstream of the masonry arch bridge, Seckin et al. (2007) performed a numerical simulation of a laboratory experiment previously conducted by Seckin and Atabay (2005) with three arch bridge models (single-span semi-circular, single-span elliptic and multi-span semi-circular arches) and one bridge model with a straight deck. The 2-D numerical energy method using HEC-RAS software estimated water surface profiles at both the upstream and downstream of the bridge as well as the afflux at the upstream with the mean error of 10% based on experimental data of Seckin and Atabay (2005). Similar to these, in reference to the UK's Boscastle flood of 2004, the water surface profiles were also examined for the particular case of vehicle blockage at an arch bridge by Xia et al., (2018). Although these studies provided an insight into the flood effects on masonry arch bridges and water surface profile results, they could not address this complex fluid-

structure interaction fully in consideration of detailed hydrodynamic, debris impact and buoyancy forces acting on the bridge. As highlighted in the manual published by Ciria (2017), a computational fluid dynamics (CFD) approach is an emerging method to assess the flood-induced loads on masonry arch bridges.

The complex interaction between flood flow with floating debris inside the flow and a masonry arch bridge can be explored at unprecedented levels of detail using an appropriate CFD approach. In CFD, the fluid domain is discretised into a series of computational points which can be either fixed, called Eulerian, or moving with the fluid, termed Lagrangian. These Eulerian and Lagrangian approaches are known as mesh-based and meshless CFD methods, respectively. Different mesh-based methods (finite difference, finite element and finite volume methods) have been implemented to evaluate the hydrodynamic loads on other bridge forms and associated decks and piers (Huang and Xiao, 2009; Erduran et al., 2012; Hartana et al., 2013; Chu et al., 2016; Oudenbroek et al., 2018; Kahraman et al., 2019; Nasim et al., 2019) where the motion of the free surface in time within the grid cell is tracked using a volume-of-fluid (VOF) method. It is clear that this mesh-based method suffers from the demand of simulating the two phases which in turn requires the interface tracking of the VOF approach(Andersson et al., 2011; Shadloo et al., 2016). Also, regarding the aim of the research presented in this paper, these studies do not include the detail of modelling free-surface flow carrying floating debris around a bridge which can be a significant challenge for mesh-based methods. Contrary to the aforementioned mesh-based methods, the meshless CFD method, smoothed particle hydrodynamics (SPH), has also been employed in engineering problems which include fast-dynamic flows, large deformations of the fluid domain with a complex free surface, motions of a floating body and the interfaces between the bodies(Gomez-Gesteira et al., 2010; Khayyer et al., 2018; Domínguez et al., 2021). In the SPH method, the flow is represented with moving particles where physical properties are defined. The present paper uses the SPH method due to its capability to capture the complex hydrodynamic phenomena associated with violent fluid-structure interaction without any special treatment compared to other CFD methods (Gomez-Gesteira et al., 2010; Khayyer et al., 2018).

Figure 1: Downstream elevation of a single-span masonry arch bridge in Derwent Reservoir, Derbyshire, UK (image by Eda Majtan)

The main components of a typical masonry arch bridge are the arch barrel, backfill, spandrel walls, abutments and piers (where multiple spans exist). Each structural component of a masonry arch bridge plays a crucial role in the load capacity and performance of the whole structure (Royles and Hendry, 1991). The failure modes of masonry arch bridges differ depending on loading conditions (e.g., in-plane or out-of-plane, static or dynamic), the behaviour of the structural members under these loads (e.g., arch barrel, spandrel wall, abutment, pier) and the interface mechanism between these structural members. Considering

flood-induced hydrostatic, hydrodynamic and debris impact loads in both the vertical and horizontal directions, possible failure modes, e.g., sliding and rotation of spandrel walls, transverse cracking due to hinge formation and shear and failure in tension can be observed as described by Kindij et al. (2014). Figure 1 shows cracking at the interface between the arch barrel and downstream spandrel wall, these cracks are propagating towards the spandrel. In the absence of monitoring data for this particular bridge, one possible cause of the crack formation maybe the resultant hydrodynamic force generated by the increase in the water level at the upstream of the bridge referred as to the afflux.

The wider research project, from which this paper forms a part, aims at investigating flood-induced hydrostatic, hydrodynamic and debris impact loads on a masonry arch bridge and the bridge response to these loads by means of smoothed particle hydrodynamics and finite element methods, respectively. The current paper numerically explores the flood-induced hydrostatic and hydrodynamic loads on a typical single-span masonry arch bridge where the hydraulic conditions represent a real-life flooding scenario observed in Cumbria, UK and the arch barrel of the bridge is fully submerged. The paper first provides a brief explanation of the research methodology (SPH) followed by details of the case study and parameters used. Finally, the results are discussed and possible aspects for future studies detailed.

2. NUMERICAL MODELLING OF FLOOD FLOW USING SPH

The SPH method is used herein to simulate the flood flow at a single-span arch bridge. The SPH method is based on solving the Navier-Stokes equations for mass and momentum conservation in Lagrangian form by representing the moving fluid with a set of particles which carries physical properties, e.g. density, velocity and pressure, detailed information on this can be found in a previous study by the authors, Majtan et al. (2021). To simulate the SPH models, the open-source SPH code, DualSPHysics v5.0 is used. This code has been validated for a variety of fluid-structure interactions in various engineering areas. In addition to its capability to simulate free-surface and complex fluid-structure interactions without any special treatment, the DualSPHysics code allows the use of graphics processing units (GPUs) rather than only central processing units (CPUs) in order to reduce the computational time and cost thus allowing simulation of 3-D engineering problems with large numerical domains as in work presented here.

2.1. Description of SPH Model

As previously mentioned, the work presented here forms part of wider research by the authors including experimental studies, thus the flume set-up used in the laboratory was simulated here in the numerical model with a 1:10 scale, see Figure 2(a). A representative single-span masonry arch bridge geometry was defined in accordance with the span and the rise-to-span ratio of many masonry arch bridge forms in the UK (Oliveira et al., 2010; Ebrahimi et al., 2016; Mathews and Hardman, 2017; Solan et al., 2020). The representative full-scale arch bridge had a span of 8 m, arise to span ratio of 0.25 and a streamwise width of 4 m corresponding to a single vehicular lane bridge. Thus, in the scaled bridge simulated in the numerical model has a span of 0.8 m and a streamwise width of 0.4 m (Figure 2(b)).

The flow velocity in rivers varies depending on the topographical and hydrological conditions and the nature of the river channel. Where the river flow interacts with a masonry arch bridge, as expected from fundamental theory, field data from the 2015 UK flood events reveals that fast flow can occur with the mean velocities of approximately 3.1 m/s at Pooley Bridge, 3.2 m/s at Eamont Bridge, 4.2 m/s at Brougham Bridge and 4.3 m/s at Sprint Bridge (Mathews and Hardman, 2017). To simulate hydraulic conditions during the real-life flooding scenario, the data obtained at Pooley Bridge is used in this study. Pooley Bridge is a village in the Lake District National Park in Cumbria, UK. The main watercourse running through

Pooley Bridge is the River Eamont which is the outlet from Ullswater and passes through the western edge of the village. The 16th-century three-span road bridge (also called Pooley Bridge) spanning the River Eamont was destroyed during the flood on the 6th December 2015 after the peak flow in the River Eamont. The hydrographs obtained at the Pooley Bridge gauging station were provided by Environment Agency and Cumbria County Council (2016) and the flow velocity of 3.14 m/s and an associated afflux of 0.6-0.8 m at the upstream of the bridge was predicted by Mathews and Hardman (2017). Although the present work focuses on an idealised single-span masonry arch bridge, the flow velocity recorded from the Pooley Bridge flood event will be used to represent a typical flood flow. Following Froude scaling, the mean velocity of 1 m/s (representing 3.14 m/s in the prototype) was imposed in time at the inlet with 0.27 m water depth (corresponding to 2.7 m in the prototype) as an initial condition, while the density of the fluid was extrapolated at the SPH inflow-outflow boundaries. The initial water depth was kept the same as 0.27 m in the numerical domain and at the outlet, and the mean velocity changing in time was defined at the outlet providing the same flow rate so as to obtain the afflux in the range predicted by Mathews and Hardman (2017) for Pooley Bridge. The same SPH parameters and GPU specifications adopted by Majtan et al. (2021) were used here. The simulation was run for 15 s physical time resulting in a total run time of 4 h 47 min 56 s with a total number of particles of 2,755,038.

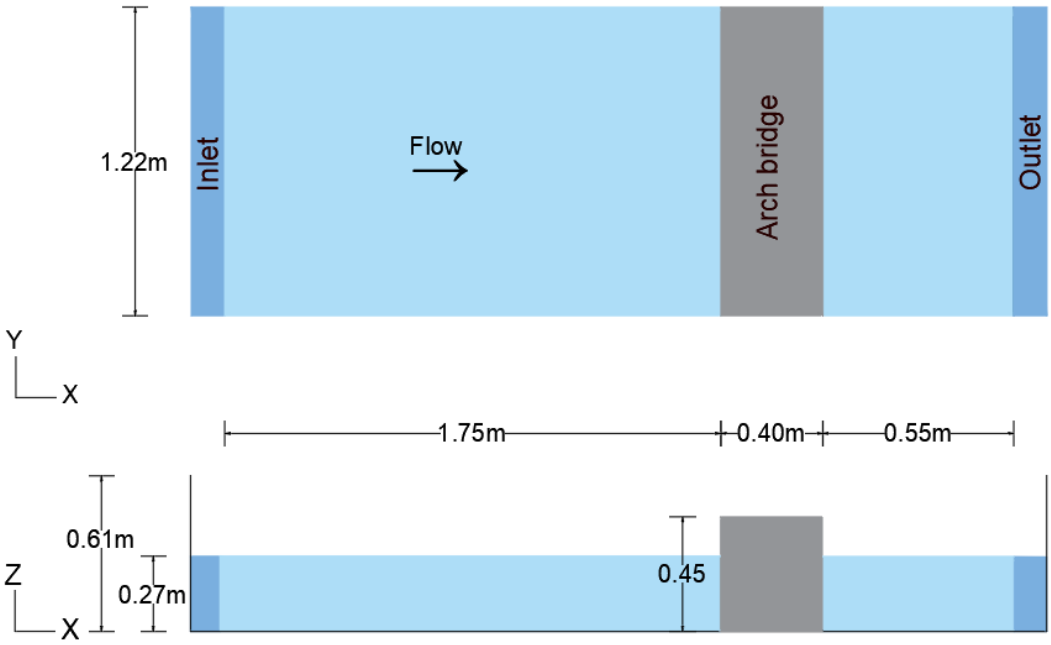

(a) Plan and side views of the numerical domain at the initial condition

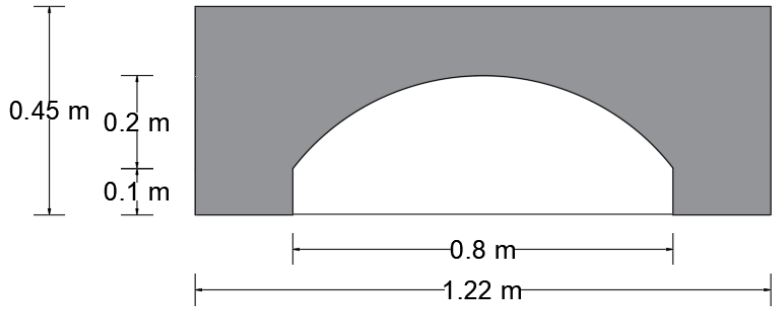

(b) Cross-section of a typical single-span arch bridge with 0.25 rise-to-span ratio

Figure 2: (a) Plan and side views of the numerical domain at the initial condition and (b) Cross-section of a typical single-span arch bridge with 0.25 rise-to-span ratio (not to scale)

2.2. Results and Discussions

Figure 3 illustrates the velocity and pressure distributions on the bridge components at t = 15 s, i.e. the abutment, arch barrel and spandrel walls where the arch barrel was fully submerged and approximately 0.066 m afflux was observed at the upstream of the bridge. The maximum velocity of 1 m/s occurred in the vicinity of the arch barrel and a negative pressure (suction) was seen at the top edge of the arch barrel (the edge of the crown) around the free-surface level with the maximum value of 0.29 kPa (290 Pa). The total pressures at the bottom of the spandrel walls were highest with 3.63 kPa and a considerable difference between the pressures on the upstream and downstream spandrel walls was observed with approximately 1 kPa due to the water depth difference and the hydrodynamic load applied on the upstream spandrel wall by the flood flow. Note that these pressure values were in the model with 1:10 scale, thus this refers to 10 kPa in the prototype. It should be also noted that despite examining the case with a fully submerged arch barrel, higher negative values might be seen on a partially submerged arch barrel depending on flow characteristics upstream and downstream of the bridge, this needs to be investigated with detailed field data.

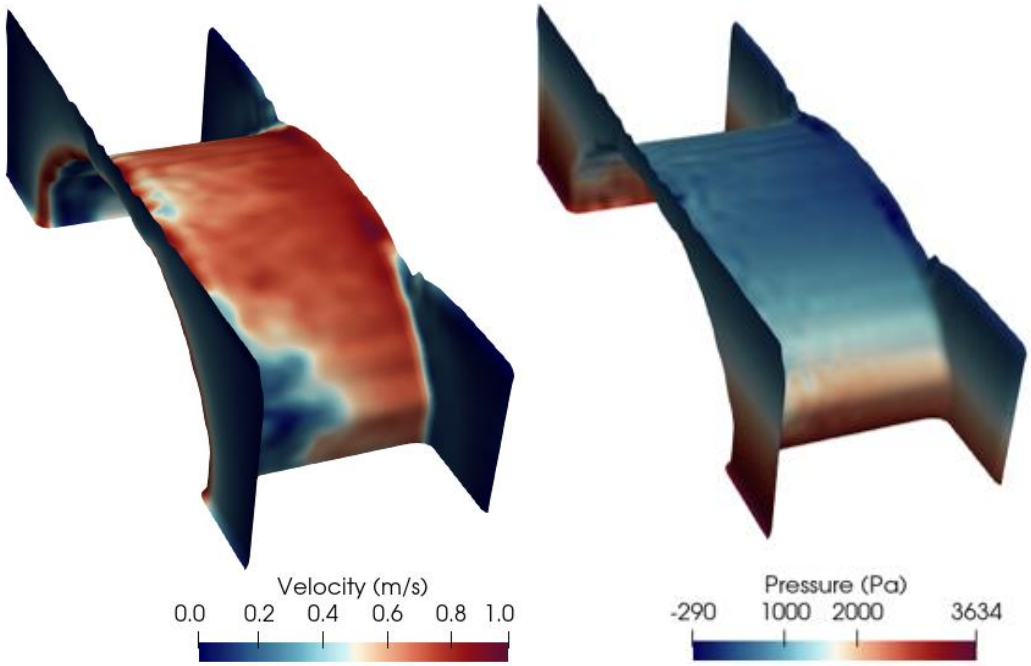

Figure 3: Velocity and pressure distributions on the bridge components at t = 15 s

The hydrodynamic pressure-time histories acting on the bridge were obtained by locating numerical pressure probes on the structural components. Figure 4(a), Figure 4(b) and Figure 4(c) show the pressure contours of the fluid particles on the upstream spandrel wall, downstream spandrel wall (including abutments) and arch barrel. The pressure probe locations are given in Table 1. Figure 5(a), Figure 5(b) and Figure 5(c) provide average pressure histories obtained on the downstream and upstream spandrel walls and the arch barrel between 12.5 s and 15 s associated with the flow in the steady state. It should be reiterated that these pressure-time histories pertain to the 1:10 scale bridge. In accordance with Froude scaling, these pressure were multiplied by a factor of 10 to represent those for the prototype.

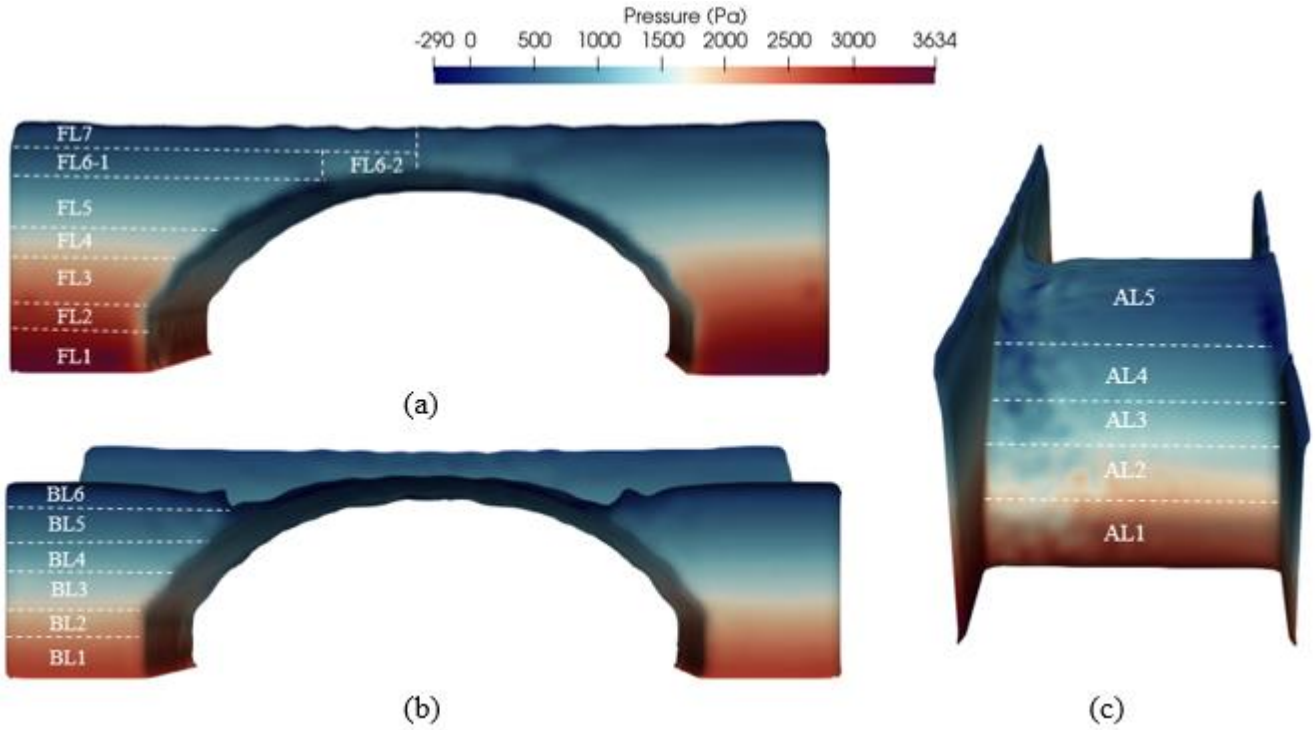

Figure 4: Pressure distribution on the scaled bridge (a) upstream, (b) downstream and (c) side view of the bridge at t = 15 s with measurement locations for detailed pressure-time histories

Table 1: Numerical probe locations at front (upstream spandrel) wall, back (downstream spandrel) wall and arch barrel for pressure measurement and associated pressure coefficients

	Name	Measurement point (x,y,z)	Pressure coefficient	Averaged pressure coefficient
Front (upstream spandrel) wall	FL1	1.75, 0.2, 0.03	0.736	0.721
	FL2	1.75, 0.2, 0.08	0.716	
	FL3	1.75, 0.2, 0.13	0.738	
	FL4	1.75, 0.2, 0.18	0.698	
	FL5	1.75, 0.2, 0.245	0.693	
	FL6-1	1.75, 0.2, 0.32	0.685	
	FL6-2	1.75, 0.59, 0.32	0.786	
	FL7	1.75, 0.2, 0.34	0.718	
Back (downstream spandrel) wall	BL1	2.15, 0.2, 0.03	-0.103	-0.117
	BL2	2.15, 0.2, 0.08	-0.122	
	BL3	2.15, 0.2, 0.13	-0.101	
	BL4	2.15, 0.2, 0.18	-0.140	
	BL5	2.15, 0.2, 0.23	-0.139	
	BL6	2.15, 0.2, 0.28	-0.098	
Arch barrel	AL1	1.95, 0.21, 0.05	0.340	0.485
	AL2	1.95, 0.24, 0.14	0.467	
	AL3	1.95, 0.31, 0.215	0.540	
	AL4	1.95, 0.42, 0.265	0.521	
	AL5	1.95, 0.61, 0.3	0.558	

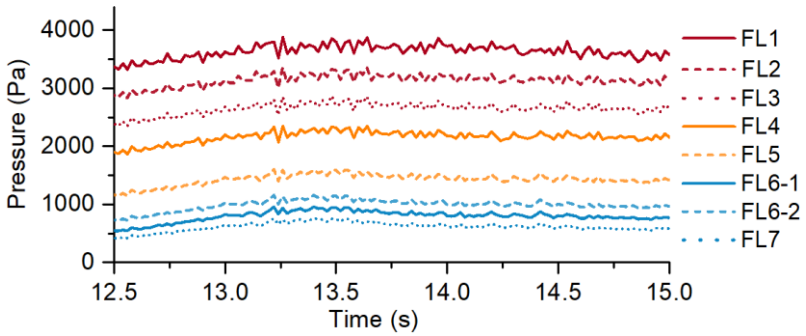

(a)

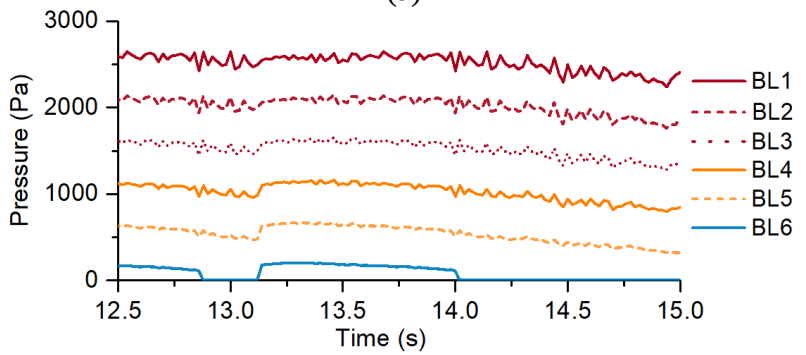

(b)

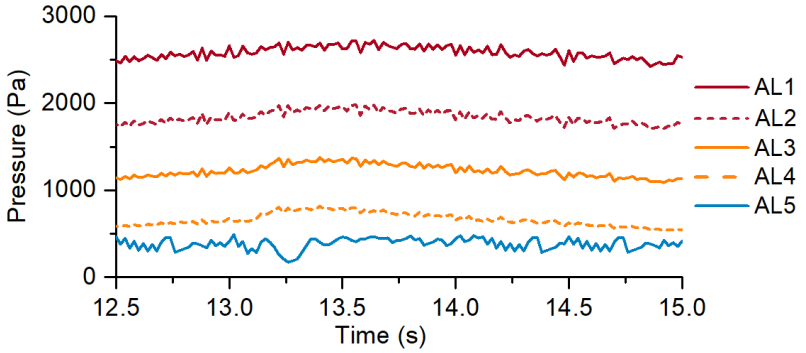

(c)

Figure 5: Pressure-time histories on (a) upstream spandrel wall, (b) downstream spandrel wall and (c) arch barrel

For better contextualisation of these results, a dimensionless number in the form of a pressure coefficient, was calculated to describe a relative pressure throughout the fluid flow field. For this, the maximum pressure values obtained at the measurement points on the scaled bridge were first multiplied by a factor of 10 considering 1:10 scale. Then, the pressure coefficient associated with the hydrodynamic load only was calculated at each measurement point by subtracting the hydrostatic pressure and the averaged pressure coefficient was obtained for each bridge component, upstream spandrel wall, downstream spandrel wall and arch barrel. The averaged pressure coefficients were highest on the upstream spandrel wall and lowest on the downstream spandrel wall with 0.721 and -0.117, respectively, while the arch barrel had a value of 0.485 (Table 1). It should be emphasised that these coefficients were measured at the specific location on the structural components, for instance the measurement point on the arch barrel was at the middle of the streamwise width which obtained positive pressures only, although negative pressure was obtained at the edge of the crown. More work is required to understand the variation of pressure coefficients with flow velocity and depth and bridge geometry.

3. CONCLUSIONS

To investigate the hydrodynamic pressures on a masonry arch bridge resulting from typical flood flows, an SPH model was developed for a single-span bridge with a fully submerged arch barrel. The afflux of 0.066 m corresponding to 0.66 m in the prototype was obtained. This increase in the water depth at the upstream as well as high hydrodynamic pressure associated with fast flow during flooding led to approximately 1 kPa maximum difference in the flood-induced loads on the upstream spandrel and downstream spandrel walls, corresponding to 10 kPa in the prototype. Considering the averaged pressure values at measurement points as well as the corresponding areas where the water interacted with the spandrel walls at upstream and downstream, the difference in the horizontal pressures led to approximately 167 kN net out-of-plane force acting to overturn the bridge in the direction of flow. In addition to this, suction pressures with the maximum value of 2.9 kPa were observed at the edge of the crown with a fully submerged arch barrel in the prototype and this may be higher when the arch barrel is partially submerged. These levels of high suction pressure may induce local damage or exacerbate damage resulting from deterioration mechanisms.

This paper has focussed on an idealised bridge geometry and flood flow considered to be representative of field conditions. Further work is required to explore the effect of variation of these parameters on the resulting hydrodynamic pressures and the implications for the structural behaviour of the masonry arch bridge.

ACKNOWLEDGEMENTS

The authors gratefully acknowledge the Ministry of National Education of the Republic of Turkey for funding this research.

REFERENCES

Andersson, B., Andersson, R., Håkansson, L., Mortensen, M., Sudiyo, R. and Van Wachem, B. (2011) *Computational fluid dynamics for engineers*. *Computational Fluid Dynamics for Engineers*.

Chu, C.-R., Chung, C.-H., Wu, T.-R. and Wang, C.-Y. (2016) 'Numerical Analysis of Free Surface Flow over a Submerged Rectangular Bridge Deck.' *Journal of Hydraulic Engineering*, 142(12) pp. 1–11.

Ciria (2017) *Manual on Scour at Bridges and Other Hydraulic Structures (C742)*. London, UK.

Deng, L., Wang, W. and Yu, Y. (2016) 'State-of-the-art review on the causes and mechanisms of bridge collapse.' *Journal of Performance of Constructed Facilities, ASCE*, 30(2) p. 04015005.

Domínguez, J. M., Fourtakas, G., Altomare, C., Canelas, R. B., Tafuni, A., García-Feal, O., Martínez-Estévez, I., Mokos, A., Vacondio, R., Crespo, A. J. C., Rogers, B. D., Stansby, P. K. and Gómez-Gesteira, M. (2021) 'DualSPHysics: from fluid dynamics to multiphysics problems.' *Computational Particle Mechanics 2021*. Springer, March, pp. 1–29.

Ebrahimi, M., Kripakaran, P., Djordjevic, S., Tabor, G., Kahraman, R., Prodanović, D. and Arthur, S. (2016) 'Hydrodynamic Effects of Debris Blockage and Scour on Masonry Bridges: Towards Experimental Modelling.' *Scour and erosion : Proceedings of the 8th International Conference on Scour and erosion (Oxford, UK, 12-15 September 2016)*, (Rssb 2005).

Ebrahimi, M., Kripakaran, P., Prodanović, D. M., Kahraman, R., Riella, M., Tabor, G., Arthur, S. and

Djordjević, S. (2018) ‘Experimental Study on Scour at a Sharp-Nose Bridge Pier with Debris Blockage.’ *Journal of Hydraulic Engineering*, 144(12) p. 04018071.

Environment Agency and Cumbria County Council (2016) *Pooley Bridge Flood Investigation Report*.

Erduran, K. S., Seckin, G., Kocaman, S. and Atabay, S. (2012) ‘3D numerical modelling of flow around skewed bridge crossing.’ *Engineering Applications of Computational Fluid Mechanics*, 6(3) pp. 475–489.

Gomez-Gesteira, M., Rogers, B. D., Dalrymple, R. A. and Crespo, A. J. C. (2010) ‘State-of-the-art of classical SPH for free-surface flows.’ *Journal of Hydraulic Research*, 48 pp. 6–27.

Hartana, Murakami, K., Yamaguchi, Y. and Maki, D. (2013) ‘2-Phase Flow Analysis of Tsunami Forces Acting on Bridge Structures.’ *Journal of Japan Society of Civil Engineers, Ser. B3 (Ocean Engineering)*, 69(2) p. I_347-I_352.

Huang, W. and Xiao, H. (2009) ‘Numerical Modeling of Dynamic Wave Force Acting on Escambia Bay Bridge Deck during Hurricane Ivan.’ *Journal of Waterway, Port, Coastal, and Ocean Engineering*, 135(4) pp. 164–175.

Hulet, K. M., Smith, C. C. and Gilbert, M. (2006) ‘Load-Carrying Capacity of Flooded Masonry Arch Bridges.’ *Proceedings of the ICE-Bridge Engineering*, 159(September) pp. 97–103.

Invernizzi, S., Lacidogna, G., Manuello, A. and Carpinteri, A. (2011) ‘AE monitoring and numerical simulation of a two-span model masonry arch bridge subjected to pier scour.’ *Strain*, 47(SUPPL. 2) pp. 158–169.

Kahraman, R., Riella, M., Tabor, G. R., Ebrahimi, M., Djordjević, S. and Kripakaran, P. (2019) ‘Prediction of flow around a sharp-nosed bridge pier: influence of the Froude number and free-surface variation on the flow field.’ *Journal of Hydraulic Research*, 1686 pp. 1–12.

Khayyer, A., Gotoh, H., Falahaty, H. and Shimizu, Y. (2018) ‘An enhanced ISPH–SPH coupled method for simulation of incompressible fluid–elastic structure interactions.’ *Computer Physics Communications*. Elsevier B.V., 232, November, pp. 139–164.

Kindij, A., Ivanković, A. M. and Vasilj, M. (2014) ‘Adjustment of small-span masonry arch bridges to present-day demands.’ *Journal of the Croatian Association of Civil Engineers*, (February 2014).

Lamb, R., Aspinall, W., Odbert, H. and Wagener, T. (2017) ‘Vulnerability of bridges to scour: insights from an international expert elicitation workshop.’ *Natural Hazards and Earth System Sciences*, 17(8) pp. 1393–1409.

Majtan, E., Cunningham, L. S. and Rogers, B. D. (2021) ‘Flood-induced Hydrodynamic and Debris Impact Forces on Single-span Masonry Arch Bridge.’ *Journal of Hydraulic Engineering*, 147(11).

Mathews, R. and Hardman, M. (2017) ‘Lessons learnt from the December 2015 flood event in Cumbria, UK.’ *Proceedings of the Institution of Civil Engineers: Forensic Engineering*, 170(4) pp. 165–178.

Nasim, M., Setunge, S., Zhou, S. and Mohseni, H. (2019) ‘An investigation of water-flow pressure distribution on bridge piers under flood loading.’ *Structure and Infrastructure Engineering*. Taylor & Francis, 15(2) pp. 219–229.

National Highways (2012) *BD 97/12 : The assessment of scour and other hydraulic actions at highway structures*. *Design Manual for Roads & Bridges*.

Oliveira, D. V., Lourenço, P. B. and Lemos, C. (2010) ‘Geometric issues and ultimate load capacity of masonry arch bridges from the northwest Iberian Peninsula.’ *Engineering Structures*, 32(12) pp. 3955–3965.

Oudenbroek, K., Naderi, N., Bricker, J. D., Yang, Y., van der Veen, C., Uijttewaal, W., Moriguchi, S. and

Jonkman, S. N. (2018) ‘Hydrodynamic and debris-damming failure of bridge decks and piers in steady flow.’ *Geosciences (Switzerland)*, 8(11).

Parola, A. C., Apelt, C. J. and Jempson, M. A. (2000) *NCHRP Report 445: Debris Forces on Highway Bridges*. *National Cooperative Highway Research Program (NCHRP) Report 445*.

Prendergast, L. J., Limongelli, M. P., Ademovic, N., Anžlin, A., Gavin, K. and Zanini, M. (2018) ‘Structural Health Monitoring for Performance Assessment of Bridges under Flooding and Seismic Actions.’ *Structural Engineering International*. Taylor & Francis, 8664 pp. 1–12.

Proske, D. (2018) *Bridge collapse frequencies versus failure probabilities*.

Proske, D. and Hubl, J. (2006) ‘Historical arch bridges under horizontal loads,’ 100.

Royles, R. and Hendry, A. W. (1991) ‘Model tests on masonry arches.’ *Proceedings of the Institution of Civil Engineers*. Thomas Telford Ltd., 91(2) pp. 299–321.

Ruocci, G., Ceravolo, R. and De Stefano, A. (2009) ‘Modal Identification of an Experimental Model of Masonry Arch Bridge.’ *Key Engineering Materials*, 413–414 pp. 707–714.

Seckin, G. and Atabay, S. (2005) ‘Experimental backwater analysis around bridge waterways.’ *Canadian Journal of Civil Engineering*, 32(6) pp. 1015–1029.

Seckin, G., Haktanir, T. and Knight, D. W. (2007) ‘A simple method for estimating flood flow around bridges.’ *Proceedings of the Institution of Civil Engineers: Water Management*, 160(4) pp. 195–202.

Shadloo, M. S., Oger, G. and Le Touzé, D. (2016) ‘Smoothed particle hydrodynamics method for fluid flows, towards industrial applications: Motivations, current state, and challenges.’ *Computers & Fluids*. Pergamon, 136, September, pp. 11–34.

Solan, B., Ettema, R., Ryan, D. and Hamill, G. A. (2020) ‘Scour Concerns for Short-Span Masonry Arch Bridges.’ *Journal of Hydraulic Engineering*, 146(2) p. 06019019.

Takano, H. and Pooley, M. (2021) ‘New UK guidance on hydraulic actions on highway structures and bridges.’ *Proceedings of the Institution of Civil Engineers: Bridge Engineering*, 174(3) pp. 231–238.

Tubaldi, E., Macorini, L. and Izzuddin, B. (2016) ‘Safety of masonry arch bridges against flood.’

Tubaldi, E., White, C. J., Patelli, E., Mitoulis, S. A., Almeida, G. De, Brown, J., Cranston, M., Hardman, M., Koursari, E., Lamb, R., Mcdonald, H., Mathews, R., Newell, R. and Pizarro, A. (2021) ‘Invited perspectives : challenges and future directions in improving bridge flood resilience.’ *Natural Hazards and Earth System Science*, (October) pp. 1–21.

Witzany, J. and Cejka, T. (2007) ‘Reliability and failure resistance of the stone bridge structure of Charles bridge during floods.’ *Journal of Civil Engineering and Management*, 13(3) pp. 227–236.

Xia, J., Teo, F. Y., Falconer, R. A., Chen, Q. and Deng, S. (2018) ‘Hydrodynamic experiments on the impacts of vehicle blockages at bridges.’ *Journal of Flood Risk Management*, 11 pp. S395–S402.